ISSN 1648-4142 / eISSN 1648-3480

VILNIUS TECH Vilnius Gediminas Technical University

TRANSPORT

2023
Volume 38
Issue 1
Pages 44-51
https://doi.org/10.3846/transport.2023.19084

Original Article

EVALUATION OF FILLET WELDS PROPERTIES PERFORMED BY COLD METAL TRANSFER ROBOTIC METAL ACTIVE GAS WELDING TECHNOLOGY

Janette BREZINOVÁ, Ján HAŠUĽ✉

Dept of Technology, Materials and Computer Supported Production, Technical University of Košice, Slovakia

Highlights:

- evaluation of the quality of corner welds used in the production of rear seats of passenger cars;
- the procedure for producing caps by Metal Active Gas (MAG) robotic welding with Cold Metal Transfer (CMT) is described;
- alternative preparations for welding inspection have been proposed;
- the quality of the welds was assessed by the visual and capillary method.

Article History:

- submitted 28 June 2022;
- resubmitted 30 November 2022;
- accepted 6 January 2023.

Abstract. The article is the result of research evaluating the quality of fillet welds used in the production of rear seat backrests for passenger cars and manufactured robotically by Cold Metal Transfer (CMT) robotic Metal Active Gas (MAG) welding. When robotizing the process, parameters such as the speed of the process itself, accuracy and quality of the welded joints are important. Dual-phase ferritic-martensitic steel HCX 590X was used for the experiment and four weld nodes were evaluated. The quality of welded joints was evaluated by visual and capillary methods. Based on the metallographic analysis, the weld depth of the weld root was evaluated. The measured values were subsequently processed by statistical method ANalysis Of Variance (ANOVA). The research confirmed that the final quality of the welds depends on the depth of the weld root weld into the Base Material (BM). This parameter has the greatest effect on the welds made and results in the entire product being taken out of service.

Keywords: metal active gas (MAG) welding, robotic, automotive industry, root penetration, microhardness.

✉Corresponding author. E-mail: *jan.hasul@gmail.com*

Notations

ANOVA – analysis of variance;
BM – base material;
CMT – cold metal transfer;
CO_2 – carbon dioxide;
HAZ – heat affected zone;
MAG – metal active gas;
Nd:YAG – neodymium-doped yttrium aluminium garnet;
WM – weld metal.

Introduction

Nowadays, governments are changing the environmental policies to reduce CO_2 emissions. Thus, one of the main measures is the reduction of fossil consumption. This directly influences industries as transports and automotive industry. Therefore, there is a need of reducing the vehicles weight, but still guaranteeing a similar or even better performance. The increasing demand for lightweight has driven automakers to apply dissimilar materials to automotive body fabrication in the automotive industry. Welding and riveting are the prominent joining processes for dissimilar materials in the vehicle body. Welded joints are commonly used in transports and automotive industry because of several advantages with respect to other joining and manufacturing techniques (Fernandes *et al.* 2017; Benedetti *et al.* 2013):

- no flanges or parts overlap is needed in contrast to bolted joints, resulting in lighter construction and materials savings;
- components of complex shapes can be obtained by joining simpler mechanical details, thus reducing machining time and costs as well as material waste;
- welding can be done in situ where the component must be installed, thus facilitating the transportation of large civil infrastructures.

Dual-phase steels are characterized by a high strength and a high ductility, which are excellent characteristics for structural design in the automotive industry. Currently, due to these characteristics and since thin sheets are possible, dual-phase steels are the most consumed steels in the automotive industry to produce a car body (Fernandes *et al.* 2017; Benedetti *et al.* 2013). Welding technology is employed as the main method for fabricating numerous products such as ships, automobiles, trains, bridges, and others. For example, the assembly process in the automotive industry essentially involves the joining of various components. During the manufacture of the car parts, the welding deformation is mainly caused by the high temperature in the welding process. Therefore, in the actual welding process, the welding deformations can lead to dimensional problems. These deformations can have a negative influence of the accuracy of fabrication and external appearance. In addition, this does not only degrade the performance of welded structures but also increases the cost of fabricated structures. Laser welding systems have been used in the automotive industry mainly due to its superiority regarding conventional processes. It has many advantages, including smaller HAZs in comparison with spot welding, higher energy efficiency and higher speed of process. In addition, laser welding process is less sensitive to comparison that spot weld processes and a wide variety of different steels grades have been successfully welded by laser welding (Lee *et al.* 2018; He *et al.* 2022). With further development of modern laser sources, the number of industrial laser applications is continuously growing. Classical laser welding, remote laser welding, cutting with scanner optics and laser brazing are well known industrial applications. The current trends for laser applications also ten to specific functionalizing of materials and surfaces properties, like local hardening of softening of components, depending on the specified component requirements. Modern high brightness laser sources like disc or fibre lasers with best beam quality are available in the multi kilowatt power region and high efficiency laser concepts like direct diode lasers have reached wall plug efficiencies in the order of magnitude of 40%. This means an improvement of a factor greater than compared to a conventional lamp pumped solid state Nd:YAG laser (Graudenz, Baur 2013).

With increasing requirement of service reliability, some key components of cars call for higher mechanical performance, especially the fatigue reliability and corrosion resistance for the welded structures. The fatigue mechanism of the metallic components with welded joints is an important scientific issue, because welding process can cause an obvious loss of fatigue strength. For the metallic component, the fatigue crack often initiates from the site that suffers a high stress concentration and therefore the fatigue crack usually starts from the weld toe of the welded metallic component, at which the change of weld surface geometry causes obvious stress concentration. Slag inclusion, porosity, inhomogeneous microstructure, and various cracks represents a serious problem in terms of structural integrity and is one of the most common causes of failure, especially in the case of welded structures, Because of heterogeneous nature of welded joints, comprising zones with different microstructures and mechanical properties, there is a significant difference in fatigue crack growth depending on welded joint geometry and crack location. Results obtained by experiments, were also used to develop numerical models, considering the heterogeneity of welded joints, i.e., at least three different zones, BM, WM and HAZ in between (Sedmak *et al.* 2021; Mlikota *et al.* 2017; Božić *et al.* 2018; Sedmak 2019). The Figure 1 shows the stages of CMT process (Sedmak *et al.* 2021).

MAG welding is a fusion method, indicated in the drawing according to ISO 4063:2009 standard. The heat source is an electric arc that burns between the end of the melting electrode and the BM in the protective active gas. In the MAG welding, gas is actively involved in metallurgical welding processes. The active gas used in the MAG welding process is CO_2, which has the strongest oxidizing effect. In the electric arc, metal vapours from the base and filler materials are ionized primarily and dissociation and ionization of the shielding gases occur secondarily. The degree of dissociation depends on the temperature of the process. Complete dissociation occurs at 6500 K, which is 6226.85 °C. Oxidation processes take place in the liquid metal. These take place more intensively in the electric arc than in the molten WM. In these processes, the elements are burned depending on the affinity for oxygen. According to this parameter, the elements in the additive materials can be divided into active – fast reacting (C, Zr, Ti, Al, V, Si, Mn) and stable – slow reacting (Fe, Cr, Mo, Ni). The advantages of the technology include high welding productivity, easy arc ignition, high desoldering performance, low equipment costs, the possibility of robotization, the possibility of welding in all position and more. Disadvantages include the susceptibility of welds to the formation

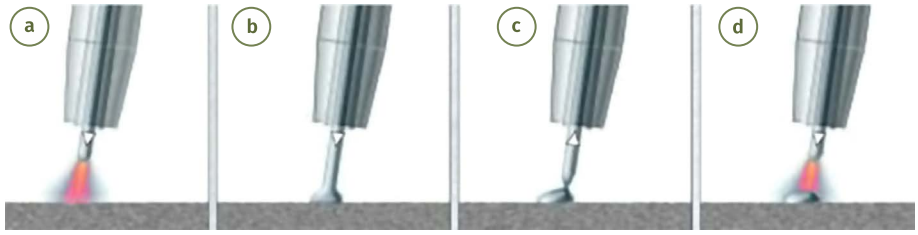

Figure 1. Process of CMT technology: (a) – arc ignition; (b) – short arc phase wire extension; (c) – wire inversion; (d) – arc re-ignition

of defects (leaks), the formation of hazardous fumes, gases harmful to humans and others. The method is used mainly in the automotive industry, aerospace industry, structural welding, shipbuilding and more (Sedmak 2019; Babčanský 2019). Due to the high requirements for precision and efficiency, many industrial robots were used in the welding industry (Xu, Wang 2021). Pulse current sources are mostly used in robotic pulse MAG welding. When welding with a pulse source, there is a rapid transition from elementary current to pulse current. The task of the elementary current is to stabilize the arc without metal transfer. The pulse current is at the level of the limit value and the so-called pinch effect occurs due to the electromagnetic field (Das *et al.* 2021). Subsequently, the droplet is transferred from the electrode, the droplets having a regular shape and the same dimensions. Electrode desoldering is regular and controlled in the form of droplets, the frequency of droplet transmission agrees with the pulse frequency of the current (Moinuddin *et al.* 2021; Sumesh *et al.* 2018). The advantages of pulse current MAG welding include the smaller HAZ, high power input, less deformation and stress in the weld, larger wire diameter at higher welding current and others (Zhang, Chen 2021). Figure 2 shows a sequence of pulse welding, where controlled short circuits and spray-free transfer of electrode material occur (Jia *et al.* 2022).

1. Material and methods

In the automotive industry, profiles are used for the rear seat backs that have a closed square profile measuring 25.4 mm made of 1.3 m thick cold rolled dual-phase steel. Dual-phase ferritic-martensitic steel HCT 590X was used in the analysed nodes. Chemical composition and mechanical properties of HCT 590X are given in Tables 1 and 2.

Welds in the analysed nodes were created robotically by CMT robotic MAG welding technology. CO_2 working gas and inert (protective) gas Ar in the ratio CO_2/Ar = 82%/18% were used. G3Si1 welding wire with a diameter of 1.0 mm was used as an additional material for all types of welds, intended for welding fine-grained steels with a minimum Re up to 470 MPa. The chemical composition of the additional material is given in Table 3.

The parameters of MAG welding process are given in Table 4.

Several principles apply to fillet *T*-welds. According to the first principle, the remelting of the welding arm must be at least $0.1 \times T_1 \leq$ penetration depth $\leq T_2$. In the second principle, the welding of the weld sides in dimension T_1 and L_1 must reach min. 70% of dimension $T_1 \rightarrow$ melting along the edge. In the third principle, the welding of the weld sides in dimension T_2 and L_2 must reach min. 70% of dimension $T_2 \rightarrow$ melting along the edge. The monitored parameters of fillet welds are shown in Figure 3.

Table 1. Chemical composition of HCT 590X

Element	C	Si	Mn	P	S	Al	Cr + Mo	Nb + Ti	V	B
Weight [%]	0.150	0.750	2.500	0.040	0.015	1.500	1.400	0.150	0.20	0.005

Table 2. Mechanical properties of HCT 590X

Tensile strength [MPa]	590
Yield strength [MPa]	550
Ductility [%]	12

Table 3. Chemical composition of additional material G3Si1

Element	C	Mn	Si	Fe
Weight [%]	0.07	1.40	0.85	–

Table 4. Parameters of the MAG welding process

Voltage [V]	Current [A]	Gas consumption [ltr/min]	Wire feed speed [m/min]	Welding power [kg/h]	WM recovery [g/100 g]
18...32	80...300	18	2.7...15.0	1.0...5.6	96

Table 5. Limit values of parameters of weld nodes

	Weld node							
	316		317		336		339	
	min	max	min	max	min	max	min	max
T_1 [mm]	1.30	1.45	1.30	1.45	1.30	1.45	1.30	1.45
T_2 [mm]	1.30	1.45	1.30	1.45	1.30	1.45	1.30	1.45
AT [mm]	0.92	–	0.94	–	0.97	–	0.99	–
GAP [mm]	0.00	0.66	0.00	0.67	0.00	0.69	0.00	0.71
L_1 [mm]	1.32	–	1.34	–	1.38	–	1.42	–
L_2 [mm]	1.32	–	1.34	–	1.38	–	1.42	–
Z_1 [mm]	0.13	2.24	0.13	2.28	0.14	2.35	0.14	2.41
Z_2 [mm]	0.26	2.29	0.13	2.36	0.14	2.28	0.14	2.29
ROOT [mm]	0.13	–	0.13	–	0.14	–	0.14	–

Welding nodes 316, 317, 336 and 339 were selected and tested for the experiment. Welding nodes are shown in Figure 4.

The quality of the created test welds was evaluated by visual inspection in the sense of the ISO 17637:2016 standard and the ISO 23277:2015 standard penetration test for non-destructive capillary testing. Weld errors were assessed within the requirements for weld quality in the sense of ISO 5817:2023 standard. The microhardness of welded joints was measured by the Vickers method on transverse metallographic cuts in the sense of ISO 9015-2:2016 standard. Microhardness was evaluated in the weld area and in the HAZ. A 4-sided pyramid with an angle of 136° was used, the load force was 0.9807 N and the load time was 15 s. To determine the strength of fillet welds, a modified static tensile test at room temperature in accordance with ISO 6892-1:2019 standard was designed. The test specimens were cut to 8 mm. The test was performed on a TIRA TEST 2300 device. Two jig alternatives in the CAD system were proposed, which enabled the clamping of samples so that the welded joints were stressed in uniaxial tension. During the metallographic analysis, the parameters were monitored according to internal standards, as in Figure 5.

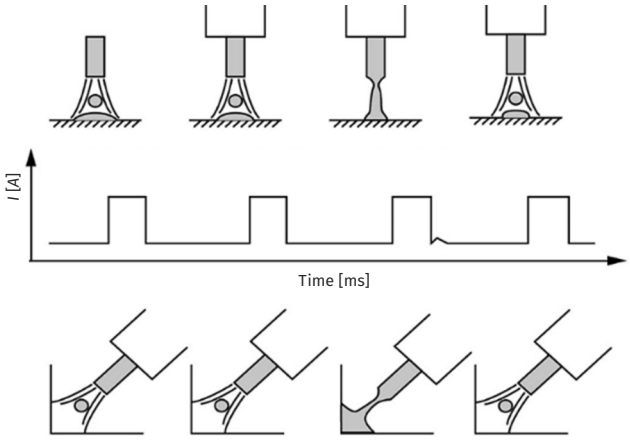

Figure 2. Sequence of pulsed robotic MAG welding

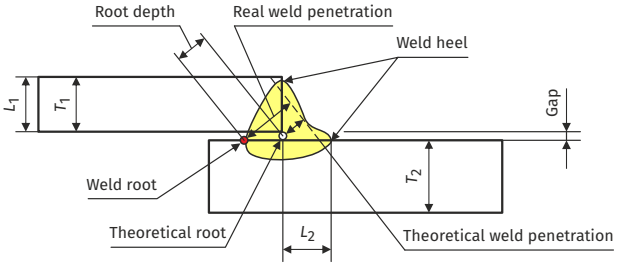

Figure 3. Monitored parameters of fillet welds

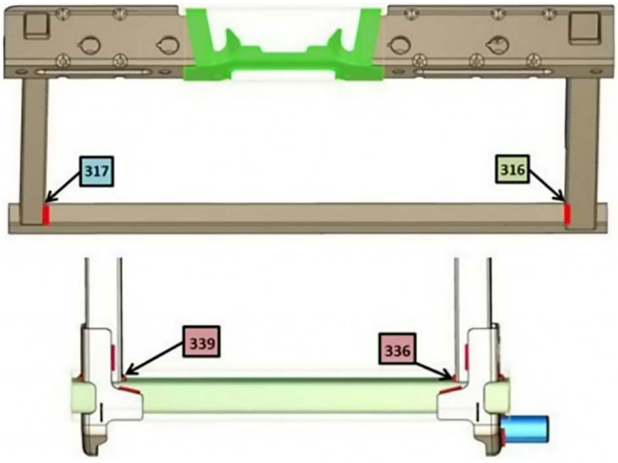

Figure 4. Examined and tested weld nodes

In Table 5, the minimum and maximum values admissible for a given weld are highlighted in colour, which is always defined by the customer based on his requirements. If the max value is not defined, only the min value is requested by the customer. The monitored parameter was the depth of boiling of the weld root, which had to reach a value in the range from 0 to 0.14 mm. The quality of the statement was then evaluated according to this dimension. The depth of boiling of the weld root into the BM as the only parameter showed regular deviations from the allowable values.

2. Results and discussion

The microhardness of the BM and the microhardness of the weld area were evaluated by the Vickers method (HV 0.1). Measurements were made at 5 points for the BM and for the weld area. It was found that the hardness of the weld showed slightly higher values than the hardness of the BM. The microhardness values for the BM are given in Table 6. The values of microhardness for the area of welds are given in Table 7.

During the creation of welds in the robotic welding process, the following errors may occur in the welds: the formation of pores in the WM, bad position of the weld caused by wear of the preparation, bad geometry of the

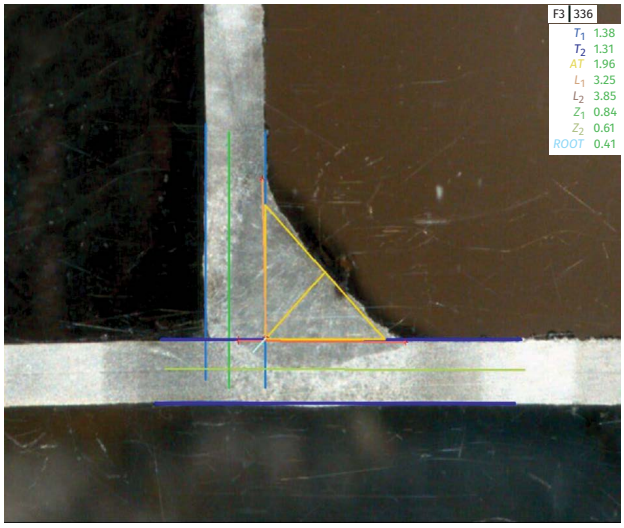

Figure 5. Monitored weld parameters – transverse metallographic cutting: T_1 – thinner BM; T_2 – thicker BM; *AT* – weld height; L_1 – weld length in T_1; L_2 – weld length in T_2; Z_1 – penetration (weld) to T_1; Z_2 – penetration (weld) to T_2; *ROOT* – weld root

preparation, poorly designed tolerance band of components at the welding point, occurrence of burns or holes in the weld caused by the wrong position of the torch, incorrect welding direction, high welding parameters, interrupted welding as a result of high welding speed, low wire feeding speed, contaminated BM, incorrect wire feeding in the feeder system, insufficient length of the weld caused by incorrect robot settings by the programmer, incorrect welding parameters, incorrect weld geometry, insufficient penetration and therefore weld strength. To determine the strength of welds, a modified static tensile test for welded joints was designed and implemented. Two types of jigs were designed to hold the samples:

- in the first proposed jig (Figure 6a), the vertical part of the sample was clamped only with mechanical pliers. In this case, the sample was released immediately after the start of the test. This problem was partly solved by welding the steel sheet to the vertical part of the sample. Despite this solution, there was a strong plastic deformation of the sample due to the deformation of the material through the slit of the jig. Immediately in the first measurement, there was a visible deformation on the jig, where the lower part of the jig mounted in mechanical pliers;
- in the second case (Figure 6b), the jig was designed so that the hydraulic tongs of the shredder gripped the sample, thus ensuring a strong and firm grip on the vertical part of the sample. After centering the machine, deformation of the sample was again visible, which led to damage of the preparation and the sample. The strength of fillet welds could not be evaluated by this test.

The dimensions of the test welds were determined based on the cross-sectional metallographic section given above in the methodology. 25 metallographic sections were made for each weld node and the dimensions of the welds were subsequently measured macroscopically. The basic criterion for a suitable weld was the penetration depth of the weld root. Figure 7 shows an example of a satisfactory (Figure 7a) and unsatisfactory (Figure 7b) weld from the weld node 339. The decisive criterion was the parameter indicating the penetration depth of the weld root. In the case of a satisfactory weld, the value of 0.14 mm was reached, and in the case of an unsatisfactory weld from this weld node, the depth of the root penetration reached the value of 0.01 mm.

Of all the prepared samples from each weld node, 26 pieces were marked as unsatisfactory welds. The minimum value to be achieved by this crucial parameter is 0.13 mm given in Table 5. The measured values of welds in the Figure 5 are given in Table 8.

Figure 8 shows an example of a satisfactory (Figure 8a) and unsatisfactory (Figure 8b) weld from the weld node 316. The decisive criterion was the parameter indicating the penetration depth of the weld root. In the case of a satisfactory weld, the value of 0.34 mm was reached, and in the case of an unsatisfactory weld from this weld node, the depth of the root penetration reached the value of 0.1 mm. The measured values of welds in the figure are given in Table 9.

Table 6. Measured values of microhardness of the BM

Basic material	Microhardness values HV 0.1					Average
1	293	234	213	240	245	245.0
2	268	272	238	284	275	267.4

Table 7. Measured values of microhardness of the area of welds

Weld node	Microhardness values HV 0.1					Average
316	270	278	297	308	285	287.6
317	333	266	245	216	286	269.2
336	209	204	201	208	212	206.8
339	242	245	261	262	247	251.4

Table 8. Measured results of weld node 339 (unsatisfactory weld)

	Weld node 339		
	min	max	measured results
T_1	1.30	1.45	1.31
T_2	1.30	1.45	1.31
AT	0.91	0.00	1.57
GAP	0.00	0.65	0.2
L_1	1.30	0.00	2.99
L_2	1.30	0.00	2.61
Z_1	0.13	2.21	0.79
Z_2	0.13	2.22	0.19
ROOT	0.13	0.00	0.01

Table 9. Measured results of weld node 316 (unsatisfactory weld)

	Weld node 316		
	min	max	measured results
T_1	1.3	1.45	1.31
T_2	1.3	1.45	1.30
AT	0.92	0	2.09
GAP	0	0.66	0.19
L_1	1.5	0	2.86
L_2	1.31	0	4.43
Z_1	0.13	2.23	0.60
Z_2	0.26	2.22	0.40
ROOT	0.13	0	0.10

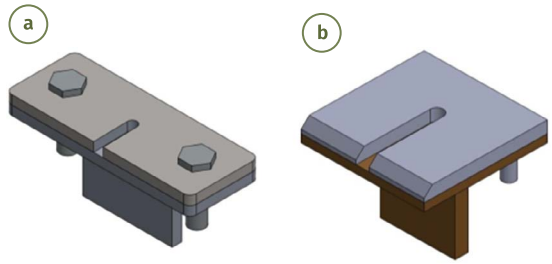

Figure 6. Proposed jigs using CAD systems: (a) – first design; (b) – alternative design

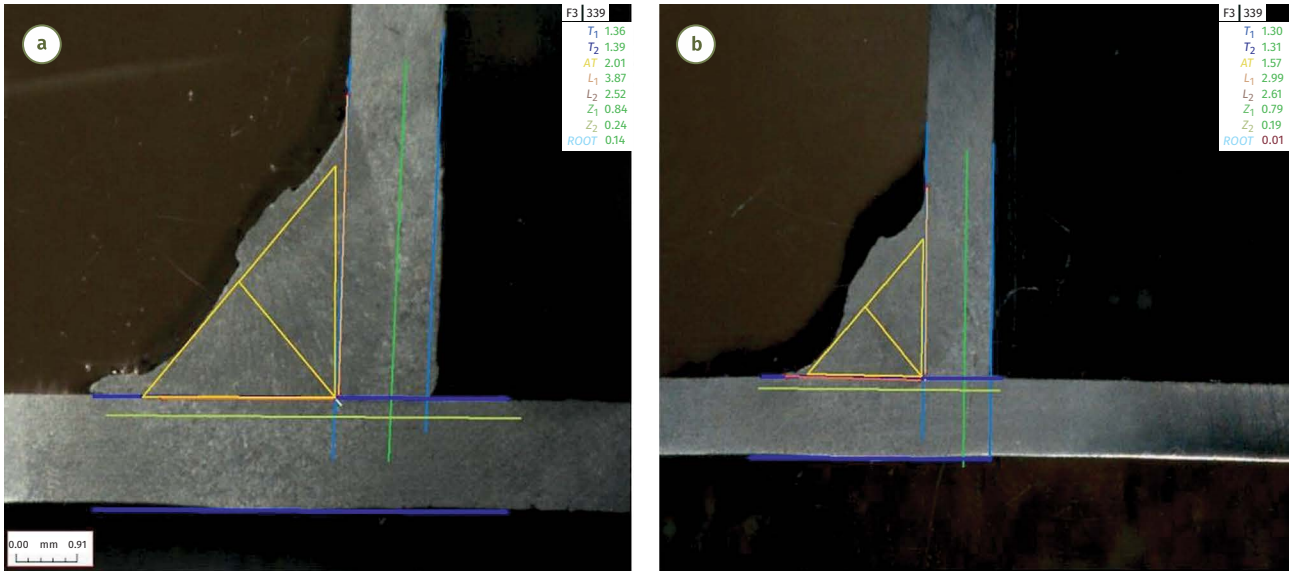

Figure 7. Comparison of satisfactory weld (a) and unsatisfactory weld (b) – weld node 339

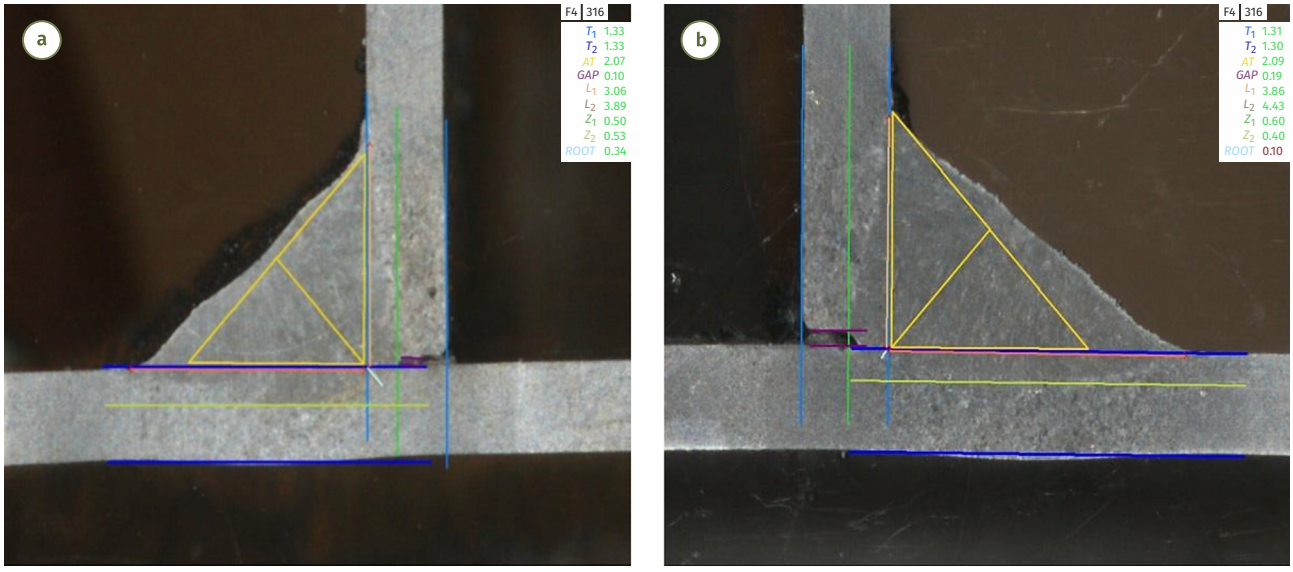

Figure 8. Comparison of satisfactory weld (a) and unsatisfactory weld (b) – weld node 316

The parameters of welded joints, which were obtained by metallographic analysis, were subjected to statistical analyses to evaluate the correlations between the values and the influence of the parameters on the dimensions of the root remelting according to the regression function was determined:

- dependence of root boiling on material welding:

$$ROOT = a + b \cdot Z_1 + c \cdot Z_2; \quad (1)$$

- dependence of root overheating on material welding length:

$$ROOT = a + b \cdot L_1 + c \cdot L_2, \quad (2)$$

where: a, b, c – coefficients.

The following weld parameters were considered:

- *ROOT* – weld root;
- Z_1 – welding (penetration) into thinner material;
- Z_2 – welding (penetration) into coarser material;
- L_1 – length of weld into thinner material;
- L_2 – length of weld into thicker material;
- *AT* – weld height.

The basic evaluation criterion was regression and correlation analysis, which consisted of 3 parts:

- output of regression analysis (Table 10);
- output of correlation analysis (Table 11);
- output from ANOVA, where the suitability of the used model was monitored (Table 12).

In the case of regression analysis, the *P*-value was compared against the level of α for individual coefficients. If the equation $P \leq \alpha$ holds, we speak of the significance of

Table 10. Regression analysis of weld nodes

	Weld node							
	316		317		336		339	
	Coefficient	P-value	Coefficient	P-value	Coefficient	P-value	Coefficient	P-value
Constant	–0.0349	0.7722	0.1381	0.0750	–0.0616	0.4714	0.1619	0.0064
Z_1	0.2452	0.0041	0.0454	0.3464	0.2506	0.0007	0.0198	0.7260
Z_2	0.1152	0.1389	0.0829	0.0412	0.1844	0.0066	0.0702	0.1247
Constant	0.2010	0.5148	0.2381	0.1045	0.2876	0.4739	–0.0072	0.9529
L_1	0.0141	0.7859	–0.0008	0.9762	–0.0129	0.8289	0.0172	0.4950
L_2	0.0111	0.8499	0.0057	0.7998	0.0112	0.8789	0.0603	0.0371

Table 11. Values of the correlation coefficient *R* for individual weld nodes

Weld node	Correlation coefficient *R*	
	Addiction to Z_1 and Z_2	Addiction to L_1 and L_2
316	0.5685	0.0651
317	0.4397	0.0610
336	0.6760	0.0794
339	0.3089	0.4115

Table 12. Significance level *F* for statistical method ANOVA

Weld node	Significance *F*	
	Addiction to Z_1 and Z_2	Addiction to L_1 and L_2
316	0.0137	0.0468
317	0.1047	0.9616
336	0.0012	0.9328
339	0.3002	0.1080

the constants for the given equation. In the results of the regression analysis, the penetration of the material (parameters Z_1 and Z_2) has a greater influence on the resulting root boiling depth (parameters Z_1 and Z_2), especially at weld nodes 316 and 336. The welding length proved to be a less important parameter for root depth.

At the value of the correlation coefficient *R*, the strong effect of welding (penetration) to thinner, respectively thicker material. In this case, the correlation coefficient *R* approached 1.

The ANOVA output used the *F*-test to verify the null hypothesis H0, where we reject H0 if $F \leq \alpha$ holds if $\alpha = 0.05$. If we reject H0, the correct choice of model applies. According to the results of ANOVA, the correct model is for the dependence Z_1, Z_2 respectively L_1, L_2 at weld nodes 316 and 336.

Conclusions

The article presents the results of a research aimed at determining the quality of fillet welds based on penetration evaluation according to the customer's requirements.

Fillet welds were made as *T*-joints and four different weld joints were evaluated. The fillet welds were evaluated by both destructive and non-destructive methods.

Visual inspection according to ISO 17637:2016 standard and capillary test according to ISO 23277:2015 standard were used as non-destructive tests. After evaluating these tests, all fillet welds were evaluated as satisfactory.

A regression and correlation analysis were performed to demonstrate the influence of material welding parameters on root depth. These showed a smaller range of root weld length to weld root depth.

During the creation of welds in the robotic welding process, the following errors may occur in the welds: the formation of pores in the WM, bad position of the weld caused by wear of the preparation, bad geometry of the preparation, poorly designed tolerance band of components at the welding point, occurrence of burns or holes in the weld caused by the wrong position of the torch, incorrect welding direction, high welding parameters, interrupted weld due to high welding speed, low wire feeding speed, contaminated BM, incorrect wire feeding in the feeder system, insufficient weld length caused by incorrect setting robot by the programmer, incorrect welding parameters, incorrect geometry of the weld, insufficient welding and therefore strength of the weld. It has been confirmed that the depth of the root of the weld in the BM has the greatest influence on the overall quality of fillet welds.

Acknowledgments

This contribution is the result of the project implementation:

- "Innovative approaches to the restoration of functional surfaces by laser weld overlaying" (APVV-20-0303);
- "The utilization of innovative technology for repair functional surfaces of mold casting dies for castings in automotive industry" (APVV-16-0359);
- "Innovation of the educational process by implementing adaptive hypermedia systems in the teaching of subjects in the field of coating technology and welding of materials" (KEGA 046TUKE-4/2022).

This support is highly appreciated by the authors.

Conflicts of interest

The authors declare no conflict of interest.

Funding

This contribution is supported by:

- "Innovative approaches to the restoration of functional surfaces by laser weld overlaying" (APVV-20-0303);
- "The utilization of innovative technology for repair functional surfaces of mold casting dies for castings in automotive industry" (APVV-16-0359);
- "Innovation of the educational process by implementing adaptive hypermedia systems in the teaching of subjects in the field of coating technology and welding of materials" (KEGA 046TUKE-4/2022).

Author contributions

Janette Brezinová – conceptualization, investigation, funding acquisition, writing (review and editing), project administration.

Ján Hašuľ – methodology, formal analysis, writing (review and editing).

All authors have read and agreed to the published version of the manuscript.

Disclosure statement

The authors thank for the financial help in the experiment Slovak Research and Development Agency (APVV) and Cultural and Educational Grant Agency (KEGA).

References

Babčanský P. 2019. *Stanovenie kvality kútových zvarových spojov v automobilovom priemysle*. Diplomová práca. Technická univerzita v Košiciach, Slovensko, 64 s. Available from Internet: https://opac.crzp.sk/?fn=detailBiblioFormChildGDKSO&sid=1207FF88EADD70B1D4C7AC0BD7FD (in Slovak).

Benedetti, M.; Fontanari, V.; Santus, C. 2013. Crack growth resistance of MAG butt-welded joints of S355JR construction steel, *Engineering Fracture Mechanics* 108: 305–315. https://doi.org/10.1016/j.engfracmech.2013.01.019

Božić, Ž.; Schmauder, S.; Wolf, H. 2018. The effect of residual stresses on fatigue crack propagation in welded stiffened panels, *Engineering Failure Analysis* 84: 346–357. https://doi.org/10.1016/j.engfailanal.2017.09.001

Das, A.; Masters, I.; Williams, D. 2021. Understanding novel gap-bridged remote laser welded (RLW) joints for automotive high-rate and temperature applications, *International Journal of Mechanical Sciences* 190: 106043. https://doi.org/10.1016/j.ijmecsci.2020.106043

Fernandes, F. A. O.; Oliveira, D. F.; Pereira, A. B. 2017. Optimal parameters for laser welding of advanced high-strength steels used in the automotive industry, *Procedia Manufacturing* 13: 219–226. https://doi.org/10.1016/j.promfg.2017.09.052

Graudenz, M.; Baur, M. 2013. Applications of laser welding in the automotive industry, in S. Katayama (Ed.). *Handbook of Laser Welding Technologies*, 555–574. https://doi.org/10.1533/9780857098771.4.555

He, Z.; Zhou, D.; Du, X.; Tao, T.; Wang, X.; Li, H.; Liu, J. 2022. Hybrid joining mechanism of rivet plug oscillating laser welding for dual-phase steel and magnesium alloy, *Journal of Manufacturing Processes* 77: 652–664. https://doi.org/10.1016/j.jmapro.2022.03.053

ISO 5817:2023. *Welding. Fusion-Welded Joints in Steel, Nickel, Titanium and Their Alloys (Beam Welding Excluded). Quality Levels for Imperfections*.

ISO 6892-1:2019. *Metallic Materials. Tensile Testing. Part 1: Method of Test at Room Temperature*.

ISO 9015-2:2016. *Destructive Tests on Welds in Metallic Materials. Hardness Testing. Part 2: Microhardness Testing of Welded Joints*.

ISO 17637:2016. *Non-Destructive Testing of Welds. Visual Testing of Fusion-Welded Joints*.

ISO 23277:2015. *Non-Destructive Testing of Welds. Penetrant Testing. Acceptance Levels*.

Jia, Y.; Wen, T.; Huang, N.; Zhang, J.; Xiao, J.; Chen, S.; Huang, W. 2022. Research on aluminum alloy welding process based on high frequency and low power pulsed laser-MIG hybrid welding, *Optics & Laser Technology* 150: 107899. https://doi.org/10.1016/j.optlastec.2022.107899

Lee, S. H.; Kim, E. S.; Park, J. Y.; Choi, J. 2018. Numerical analysis of thermal deformation and residual stress in automotive muffler by MIG welding, *Journal of Computational Design and Engineering* 5(4): 382–390. https://doi.org/10.1016/j.jcde.2018.05.001

Mlikota, M.; Schmauder, S.; Božić, Ž.; Hummel, M. 2017. Modelling of overload effects on fatigue crack initiation in case of carbon steel, *Fatigue & Fracture of Engineering Materials & Structures* 40(8): 1182–1190. https://doi.org/10.1111/ffe.12598

Moinuddin, S. Q.; Hameed, S. S.; Dewangan, A. K.; Kumar, K. R.; Kumari, A. S. 2021. A study on weld defects classification in gas metal arc welding process using machine learning techniques, *Materials Today: Proceeding* 43: 623–628. https://doi.org/10.1016/j.matpr.2020.12.159

Sedmak, A.; Hemer, A.; Sedmak, S. A.; Milović, L.; Grbović, A.; Čabrilo, A.; Kljajin, M. 2021. Welded joint geometry effect on fatigue crack growth resistance in different metallic materials, *International Journal of Fatigue* 150: 106298. https://doi.org/10.1016/j.ijfatigue.2021.106298

Sedmak, S. A. 2019. *Procena integriteta i veka zavarenih spojeva mikrolegiranih čelika povišene čvrstoće pri dejstvu statičkog i dinamičkog opterećenja*. Doktorska disertacija. Mašinski fakultet, Univerzitet u Beogradu, Republika Srbija. 219 s. Available from Internet: https://nardus.mpn.gov.rs/handle/123456789/17618 (in Serbian).

Sumesh, A.; Nair, B. B.; Rameshkumar, K.; Santhakumari, A.; Raja, A.; Mohandas K. 2018. Decision tree based weld defect classification using current and voltage signatures in GMAW process, *Materials Today: Proceedings* 5(2): 8354–8363. https://doi.org/10.1016/j.matpr.2017.11.528

Xu, Y.; Wang, Z. 2021. Visual sensing technologies in robotic welding: recent research developments and future interests, *Sensors and Actuators A: Physical* 320: 112551. https://doi.org/10.1016/j.sna.2021.112551

Zhang, H.; Chen, C. 2021. Effect of pulse frequency on weld appearance of Al alloy in pulse power ultrasonic assisted GMAW, *Journal of Manufacturing Processes* 71: 565–570. https://doi.org/10.1016/j.jmapro.2021.09.047